Denormalization of Visibilities for In-Orbit Calibration of Interferometric Radiometers

Francesc Torres, *Member, IEEE*, Ignasi Corbella, *Member, IEEE*, Adriano Camps, *Senior Member, IEEE*, Núria Duffo, *Member, IEEE*, Mercè Vall-llossera, *Member, IEEE*, Santiago Beraza, Carles Gutiérrez, and Manuel Martín-Neira, *Member, IEEE*

***Abstract*—This paper reviews the relative calibration of an interferometric radiometer taking into account the experimental results of the first batch of receivers developed in the frame of the European Space Agency's Soil Moisture and Ocean Salinity mission. Measurements show state-of-the-art baseline performance as long as the system is capable of correcting the effect of orbital temperature swing. A method to validate internal calibration during in-orbit deep-sky views and to correct linearity errors is also presented.**

***Index Terms*—Calibration, interferometry, radiometer.**

I. Introduction

SOIL MOISTURE and Ocean Salinity (SMOS) is the second Earth Explorer Mission to be developed as part of the European Space Agency's (ESA) Living Planet Program, scheduled for launch in 2007. It has been designed to observe soil moisture over the Earth's landmasses [1] and salinity over the oceans [2]. Soil-moisture data are urgently required for hydrological studies, and data on ocean salinity are vital for improving our understanding of ocean circulation patterns. SMOS' single payload is the Microwave Imaging Radiometer with Aperture Synthesis (MIRAS) [3], a dual-polarization L-band radiometer using two-dimensional (2-D) aperture synthesis. It consists of a Y-shaped interferometric radiometer formed by 69 receivers called lightweight cost-effective front end (LICEF) placed along the arms. A cross correlation of the signals collected by each receiver pair "k, j" gives the samples of the so-called visibility function V_{kj}. The brightness temperature map is then obtained by a Fourier synthesis of the calibrated visibility function. Due to the large amount of correlations, MIRAS uses one-bit two-level digital correlators. The signal collected by the antennas is downconverted to an intermediate frequency, yielding their in-phase (i_k, i_j) and quadrature (q_k, q_j) components. These signals are fed into the one-bit two-level correlators to measure M_{kj}^{ii}, M_{kj}^{iq}, M_{kj}^{qq}, and M_{kj}^{qi}. These real correlations are then combined into the so-called nominal and redundant normalized complex correlations

$$M_{kj}^{\mathrm{Nom}} = M_{kj}^{ii} + jM_{kj}^{qi} \tag{1}$$

$$M_{kj}^{\mathrm{Red}} = M_{kj}^{qq} - jM_{kj}^{iq}. \tag{2}$$

Since in an ideal instrument nominal and redundant correlations are equal, throughout the text the symbol M_{kj} is used to refer to any of them (Fig. 1). A noise injection radiometer (NIR) placed in the hub measures the scene mean temperature. The NIR, when switched to the internal noise distribution network (NDN), also acts as reference radiometer to calibrate the power measuring system (PMS) in each LICEF. The visibility

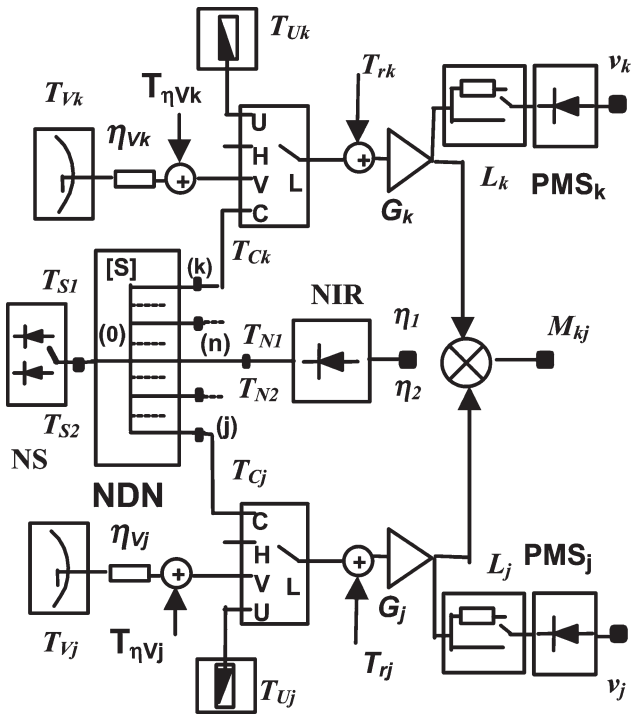

Fig. 1. Block diagram of a single baseline, compounded by two LICEF receivers (k and j) and a complex one-bit two-level correlator. Basic outputs of the system are the normalized correlations M_{kj} and the PMS voltage readings v_k and v_j, which are used to denormalize the correlations. The LICEF can be switched to the CAS, which includes a two-level NS, an NDN, and a reference radiometer called NIR. The CAS is used for internal phase and amplitude calibration of the baseline. Each LICEF can also be switched to an internal matched load (U-load) for calibration purposes. When switched to the antenna (H or V polarizations), each baseline gives a sample of the so-called visibility function V_{kj}. The definition and interrelation of all magnitudes is given in Section I.

Manuscript received September 30, 2005; revised December 20, 2005. This work was supported in part by the Spanish Ministry of Science and Technology (MCYT) and the European Union Fundao Europeu de Desenvolvimento Regional (FEDER) under Project TIC2002-04451-C02-01 and European Aeronautic Defence and Space CASA Espacio, under the Soil Moisture and Ocean Salinity Payload Module (PLM) project.

F. Torres, I. Corbella, A. Camps, N. Duffo, M. Vall-llossera, S. Beraza, and C. Gutiérrez are with the Department of Signal Theory and Communications, Universitat Politècnica de Catalunya, 08034 Barcelona, Spain (e-mail: xtorres@tsc.upc.edu).

M. Martín-Neira is with the European Space Research and Technology Center, European Space Agency, 2200 AG Noordwijk, The Netherlands.

Digital Object Identifier 10.1109/TGRS.2006.874246

samples are denormalized and corrected from instrumental errors according to

$$V_{kj} = \frac{\sqrt{T_{\mathrm{sys}_{Ak}} T_{\mathrm{sys}_{Aj}}}}{G_{kj}} M_{kj} \quad T_{\mathrm{sys}_{Ak}} = \frac{v_{Ak} - v_{\mathrm{off}k}}{G_k^A}. \tag{3}$$

The computation of normalized correlations M_{kj} and the fringe wash term G_{kj} is thoroughly detailed in [4]. Extensive experimental results to validate the calibration approach can be found in [5]. $T_{\mathrm{sys}Ak}$ ($A = V$, H polarizations) stands for system temperature referred to the antenna plane, which is obtained from PMS$_k$ reading v_{Ak}, once PMS$_k$ offset and gain at antenna plane, $v_{\mathrm{off}k}$ and G_k^A, are calibrated.

A. Two-Level Four-Point Calibration

The PMS is calibrated at plane C (Fig. 1) by means of the so-called two-level four-point method [6], [7]. HOT and WARM injected temperatures are defined at the C port as

$$T_{Ck}^{\mathrm{HOT}} = T_{S2}|s_{k0}|^2 = 1500 \text{ K} \quad T_{Ck}^{\mathrm{WARM}} = T_{S1}|s_{k0}|^2 = 75 \text{ K} \tag{4}$$

where T_{S2} and T_{S1} are the HOT and WARM temperatures injected by the noise source (NS) to port "0" of the NDN, and S_{k0} is the S parameter from port "0" to port "k" (switch-C input). Related system temperatures can be expressed as

$$\begin{aligned} T_{\mathrm{sysC}k}^{\mathrm{HOT}} &= T_{Ck}^{\mathrm{HOT}} + T_{\mathrm{ph}}^{\mathrm{NDN}} \left(1 - |s_{k0}|^2\right) + T_{\mathrm{r}k} \\ T_{\mathrm{sysC}k}^{\mathrm{WARM}} &= T_{Ck}^{\mathrm{WARM}} + T_{\mathrm{ph}}^{\mathrm{NDN}} \left(1 - |s_{k0}|^2\right) + T_{\mathrm{r}k}. \end{aligned} \tag{5}$$

The term T_{rk} stands for receiver temperature, and $T_{\mathrm{ph}}^{\mathrm{NDN}}$ is the NDN physical temperature. Two additional measurements are performed by inserting an IF attenuator L_k in the PMS path. The four-point PMS readings are then defined as

$$\begin{aligned} v_{1k} &= v_{\mathrm{off}k} + G_k^C T_{\mathrm{sysC}_k}^{\mathrm{WARM}} \quad v_{3k} = v_{\mathrm{off}k} + \frac{G_k^C}{L_k} T_{\mathrm{sysC}_k}^{\mathrm{WARM}} \\ v_{2k} &= v_{\mathrm{off}k} + G_k^C T_{\mathrm{sysC}_k}^{\mathrm{HOT}} \quad v_{4k} = v_{\mathrm{off}k} + \frac{G_k^C}{L_k} T_{\mathrm{sysC}_k}^{\mathrm{HOT}}. \end{aligned} \tag{6}$$

The PMS gain is retrieved by a differential method, which eliminates the noise contribution of the receiver and the NDN

$$G_k^C = \frac{v_{2k} - v_{1k}}{(T_{S2} - T_{S1})|S_{k0}|^2}. \tag{7}$$

Since the NIR is also measuring the HOT and WARM temperatures, PMS$_k$ gain can be computed relative to the differential temperatures measured by the NIR, $T_{N2} - T_{N1}$, placed at port "n" of the NDN (Fig. 1)

$$G_k^C = \frac{v_{2k} - v_{1k}}{T_{N2} - T_{N1}} \frac{|S_{n0}|^2}{|S_{k0}|^2}. \tag{8}$$

By doing so, the NS does not require to be calibrated. Finally, the PMS gain is translated to the antenna plane as

$$G_k^A = G_k^C \frac{|S_{LA_k}|^2}{|S_{LC_k}|^2} \eta_{A_k} \tag{9}$$

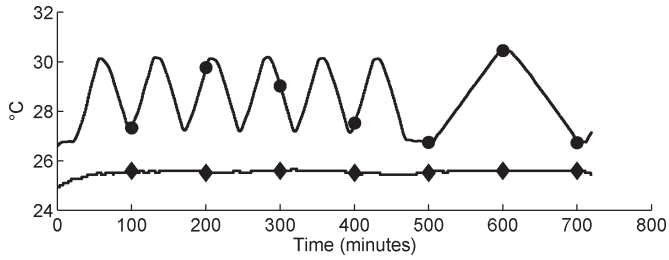

Fig. 2. Temperature-swing tests in the thermal chamber reproduce thermal evolution of the instrument along several orbits. LICEF U-load (•) and CAS NDN (♦) temperatures are continuously recorded.

where S_{LAk}, S_{LCk} are the switch S-parameters and η_{Ak} are the antenna losses. PMS$_k$ offset, which exclusively depends on PMS$_k$ linearity, is retrieved by the four-point method [4]

$$v_{\mathrm{off}k} = \frac{v_{2k} v_{3k} - v_{1k} v_{4k}}{(v_{2k} - v_{4k}) - (v_{1k} - v_{3k})}. \tag{10}$$

II. Temperature-Drift Correction on Relative Calibration

Relative (internal) calibration is performed by switching the instrument to the noise-injection mode described so far, a few times per orbit. This section is devoted to describing the procedure to compensate the effect of temperature drift in between calibration events.

The LICEF internal temperature is expected to present about 2 °C peak-to-peak drift along one orbit. In order to experimentally assess the impact of orbital temperature drift of main baseline parameters, a smooth temperature swing of about 4 °C peak to peak, with a period of 100 min, is applied during 12 h to two LICEF units labeled EM03 and EM04, which, by the time of the writing of the final revision of this manuscript, are fully representative of flight units. The two receivers are enclosed in a climate chamber, while the calibration system (CAS) is kept outside at a fairly constant temperature. A standard power meter is acting as reference radiometer (NIR). Both LICEF U-load and CAS temperature are monitored during the test (Fig. 2). The receivers are configured in calibration mode so as to continuously repeat the four-point calibration sequence in steps of 1.2 s. An additional step is used to switch to the internal matched load (U-noise injection). Therefore, PMS offset and gain is estimated every 6 s. (Fig. 3, top and bottom, respectively). PMS gain and offset at a given temperature T_{ph1} can be expressed as

$$\begin{aligned} G(T_{\mathrm{ph1}}) &= G(T_{\mathrm{ph0}}) \left(1 + \frac{S_{T_{\mathrm{ph}}}^G}{100} \Delta T_{\mathrm{ph}}\right) \\ v_{\mathrm{off}}(T_{\mathrm{ph1}}) &= v_{\mathrm{off}}(T_{\mathrm{ph1}}) + S_{T_{\mathrm{ph}}}^{V_{\mathrm{off}}} \Delta T_{\mathrm{ph}} \end{aligned} \tag{11}$$

where T_{ph0} is the LICEF temperature during calibration. The sensitivity parameters are estimated from Fig. 3 by a linear fit, yielding

$$S_{T_{\mathrm{ph}}}^{G_0} = -0.36\%/^\circ\mathrm{C} \quad S_{T_{\mathrm{ph}}}^{v_{\mathrm{off}}} = -0.42 \text{ mV}/^\circ\mathrm{C}. \tag{12}$$

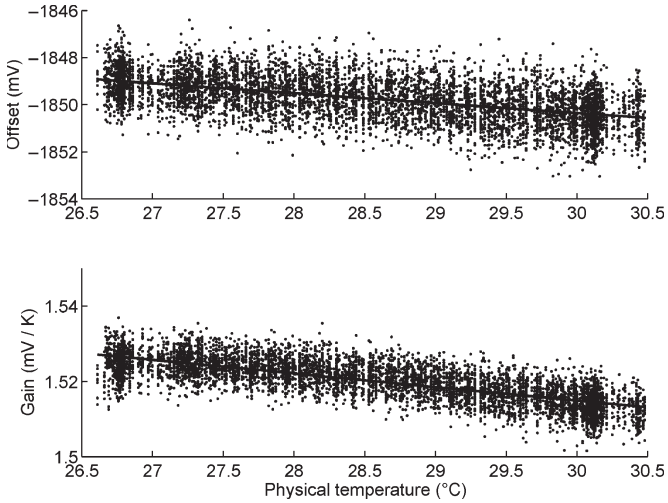

Fig. 3. EM04 PMS offset (top) and gain (bottom) sensitivity to temperature are retrieved by linear fit.

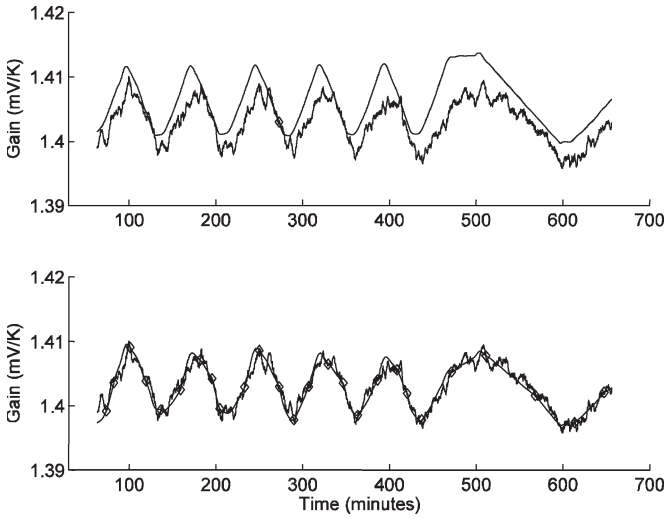

Fig. 4. Measured and predicted EM03 gain drift due to temperature swing. (Top) PMS is calibrated at one single position ($\diamondsuit$). Mean error is 0.27% with a standard deviation of 0.15%. (Bottom) Gain estimation uses four calibration points per swing. Samples in between calibration points are corrected by a linearly weighted average, yielding a mean error below 0.01% and a standard deviation of 0.08%.

Fig. 3 shows that parameter sensitivity to temperature can be retrieved by periodically running the instrument in calibration mode during a dedicated full orbit. Fig. 4 (top) gives the comparison between EM03 measured and predicted PMS-gain drift. Gain prediction makes use of a single calibration point (diamond mark), continuous temperature measurements (Fig. 2), and the sensitivity parameters computed in (11) and (12). However, this simple calibration presents a bias error, which is also very dependent on the particular calibration point. This reveals internal-temperature gradients inside the LICEF, with slightly different time constants. In order to overcome this problem, an alternative method is shown in Fig. 4 (bottom), where four calibration points per orbit are used (diamond marks). PMS gain in between calibrated points uses a linearly weighted average to achieve an outstanding track of temperature drift along the orbit.

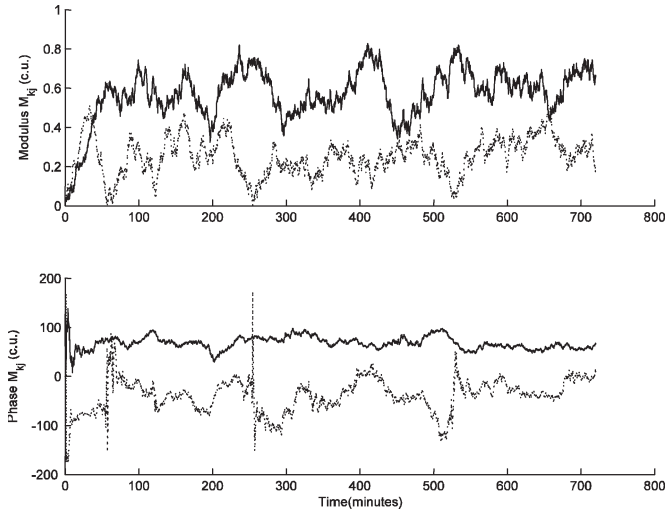

Fig. 5. (Top) Modulus and (bottom) phase of nominal (solid line) and redundant (dotted line) normalized U-mode correlations. Modulus measured in correlation units (1 c.u. $= 10^{-4}$). Each point was averaged out of 300 samples at a 1.2-s integration time.

A. U-Noise Correlations

U-noise correlations are measured by switching the LICEF to the internal matched load (Fig. 1). Ideally, these correlations give a zero-mean output. However, some residual correlation is present due to noise coupling between receivers (e.g., via the common local oscillator). This residual correlation must be characterized and eliminated from all correlations. Fig. 5 shows U-noise correlations measured in correlation units (1 c.u. $= 10^{-4}$). Their mean value is 0.58 c.u. (0.24 c.u.) for the nominal (redundant) amplitude and 69° (-39°) for the phase. The standard deviation is 0.098 c.u. (0.095 c.u.) for the amplitude and 12° (32°) for the phase. The dispersion in the measurements is mainly related to temperature drift since the effect caused by finite integration time has been reduced well below 1 c.u. by averaging 300 consecutive samples at 1.2 s. As shown, it is not practical to have frequent in-orbit estimates of residual U-noise drift due to the large integration periods required to obtain each sample. Instead, residual U-noise has been constrained below 1 c.u. by proper hardware design. Then, its mean value can be well estimated by averaging at least 300 samples distributed along one orbit in calibration mode. This averages both thermal noise and temperature drift. The mean value obtained by this procedure is removed from all correlations. The error due to residual U-noise will present a zero mean with the standard deviation measured in Fig. 5, which is below 0.1 c.u.

B. Normalized Correlations

Normalized correlations when HOT or WARM noise is injected can be expressed as given in [8, eq. (9)]

$$M_{kj}^{C2} = \frac{S_{k0}S_{j0}^{*}\left(T_{S2} - T_{\mathrm{ph}}^{\mathrm{NDN}}\right)}{\sqrt{T_{\mathrm{sysC}k}^{\mathrm{HOT}}T_{\mathrm{sysC}j}^{\mathrm{HOT}}}}G_{kj} \tag{13}$$

$$M_{kj}^{C1} = \frac{S_{k0}S_{j0}^{*}\left(T_{S1} - T_{\mathrm{ph}}^{\mathrm{NDN}}\right)}{\sqrt{T_{\mathrm{sysC}k}^{\mathrm{WARM}}T_{\mathrm{sysC}j}^{\mathrm{WARM}}}}G_{kj}. \tag{14}$$

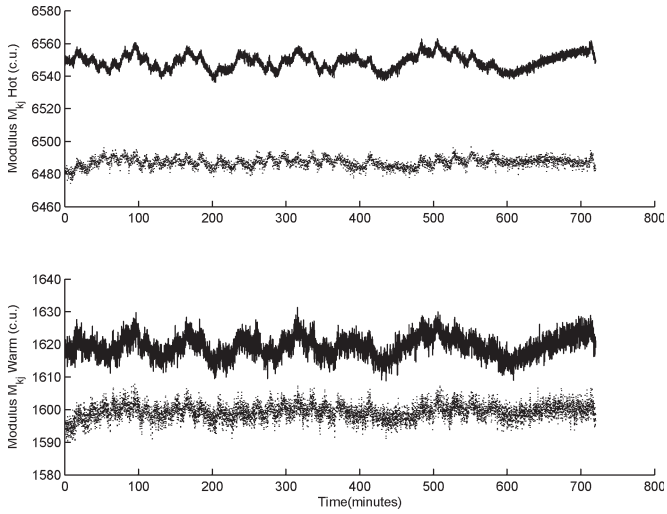

Fig. 6. Modulus of (top) HOT and (bottom) WARM normalized correlations for the nominal (dashed) and redundant (dotted) cases.

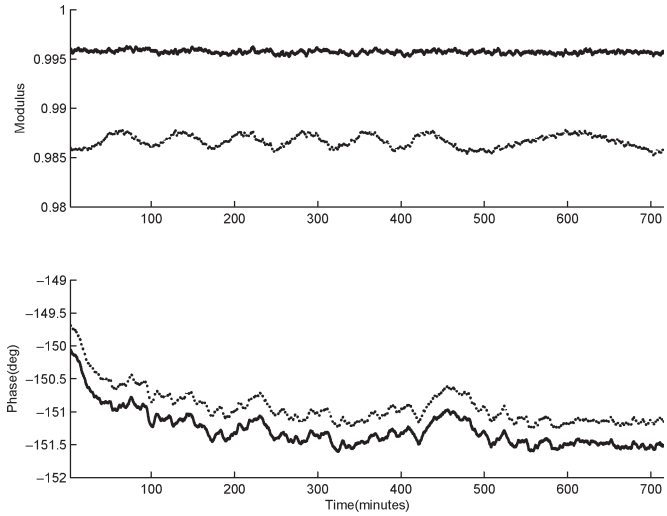

Fig. 7. EM03 and EM04 evolutions of the FWF modulus (top) and phase (bottom) at the origin. The drift is below 0.5% and 0.75°, respectively, for the 4 °C multicycle temperature swing. Note that measurements include the CAS contribution.

The NS and the NDN are placed outside the climate chamber at a fairly constant temperature (Fig. 2). Therefore, the temperature drift on measured normalized correlations is exclusively caused by LICEF and correlator temperature variations. Fig. 6 (top) shows the amplitude of HOT normalized correlations giving a mean value of 6549 c.u. (6487 c.u.) for the nominal (redundant) case, with standard deviation of 0.07% (0.05%). Fig. 6 (bottom) shows the amplitude of WARM noise injection, which gives a mean value of 1619 c.u. (1599 c.u.) with standard deviation of 0.21% (0.16%). There is a small undesired difference between the mean of nominal and redundant correlations of 0.95% and 1.25% on the HOT and WARM cases, respectively. These discrepancies are attributed to slight differences on the equivalent receiver noise temperature and end-to-end frequency response for the in-phase and quadrature channels of each receiver. The drift on normalized correlations is mainly contributed by receiver temperatures $T_{\mathrm{r}k}$, $T_{\mathrm{r}j}$ drift. This conclusion is based on the fact that normalized correlations are insensitive to gain changes. Additionally, the fringe washing function (FWF) term G_{kj}, as will be shown in the next section, is also very insensitive to temperature drift. Conventional measurements by MIER Espacio give 0.5 K/°C and 1 K/°C for the EM03 and EM04 receiver temperature sensitivity, respectively, which is in good concordance with measured amplitude ripple on normalized correlations (Fig. 7).

It is also worth to comment that the phase of nominal correlations presents a constant 0.3° difference between the HOT and WARM cases (0.1° in redundant correlations) along the whole test. This is assigned to a slight compression of the HOT signal (amplitude-to-phase conversion). The case in [5, Fig. 6] clearly shows this effect.

C. Fringe Washing Function

As shown in (3), the FWF, evaluated at the origin, is required to calibrate each sample of the visibility function. The FWF term is calculated by combining (3) and (8) into (13) and (14) to yield (15), shown at the bottom of the page.

This resulted in a very robust estimation of the FWF since it exclusively depends on normalized correlations and PMS linearity. Note that the two-level differential approach eliminates the dependence on physical temperature of the NDN, which is very difficult to measure and model. The FWF term presents a mean nominal (redundant) value of 0.996 (0.987). This high value confirms that end-to-end frequency response between units is very similar. There is a difference of 0.9% between the nominal and redundant amplitudes (0.35° phase difference), assigned to a slight difference between the in-phase and quadrature frequency response of the receivers. The standard deviation due to thermal drift in the nominal (redundant) case is 0.02% (0.06%). The FWF phase is also very insensitive to thermal drift, yielding a standard deviation for the nominal (redundant) case of 0.27° (0.28°).

D. Denormalized Visibility

Finally, denormalized visibilities are computed by means of (3). Fig. 8 gives the amplitude error after denormalizing HOT correlations. Temperature drift has only been corrected for PMS gain (dominant error), according to the estimation given in Fig. 4 (bottom). A slight dependence with temperature is still clearly seen, probably due to PMS offset drift (Fig. 9 top). Fig. 8 (top) gives the error when an averaging factor of 16 has been applied to all measurements, whereas Fig. 8 (bottom) shows the

$$G_{kj}^{C} = \frac{M_{kj}^{C2}\sqrt{(v_{2k}-v_{\mathrm{off}k})(v_{2j}-v_{\mathrm{off}j})} - M_{kj}^{C1}\sqrt{(v_{1k}-v_{\mathrm{off}k})(v_{1j}-v_{\mathrm{off}j})}}{\sqrt{(v_{2k}-v_{1k})(v_{2j}-v_{1j})}} \tag{15}$$

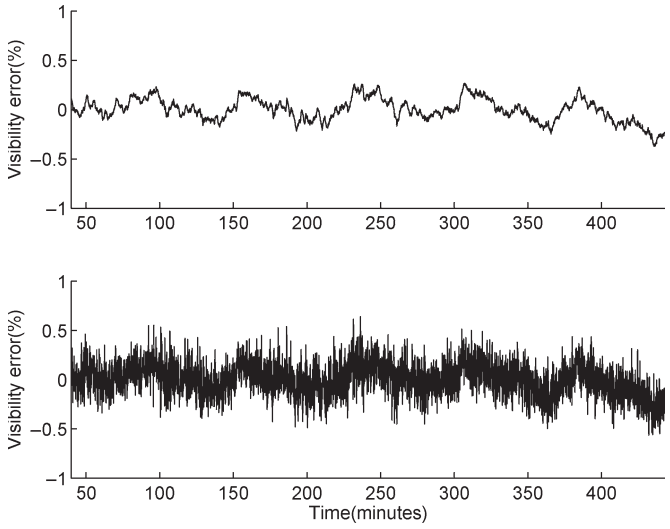

Fig. 8. HOT noise-injection visibility error after PMS-gain correction for temperature drift. Its mean value is 958.4 K. The standard deviation is 0.08% when (top) an averaging factor of 16 is applied and (bottom) 0.12% at a nominal integration time of 1.2 s.

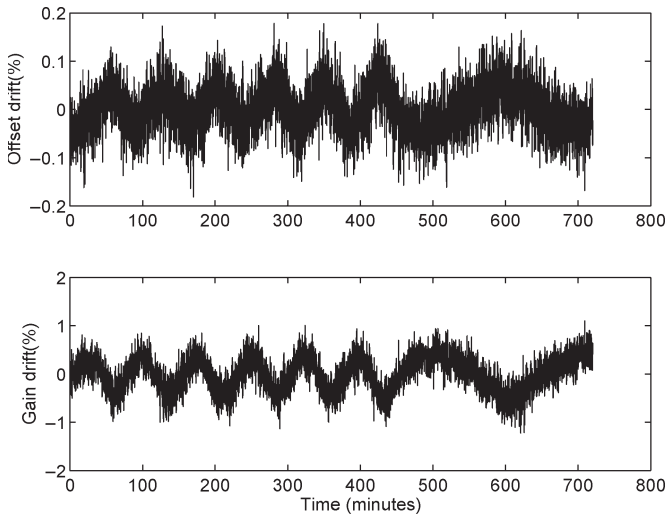

Fig. 9. EM04 PMS offset (top) and gain (bottom) drift. PMS parameters are retrieved by the four-point method. HOT and WARM noise temperatures estimated from noise source ENR and NDN S-parameters.

case when the averaging factor has only been applied to estimate PMS-gain drift (calibration mode). That is, denormalized HOT visibility is displayed, after correction, with the nominal 1.2-s integration time (imaging mode). As shown, amplitude error due to temperature drift for in-orbit calibrated visibilities is well below the 1% target, even in the case that a 4 °C peak-to-peak temperature swing is present.

III. MIRAS–SMOS Absolute Calibration

The previous section was devoted to relative calibration in the sense that PMS calibration of all receivers was referred to the differential measurement of injected noise performed by the NIR [9]. Additionally, temperature correction was performed to compensate deviation from relative calibration. This section is devoted to present the procedure and validation test devoted to the absolute calibration of the instrument.

Absolute calibration of the MIRAS–SMOS instrument is performed by periodic (e.g., monthly) deep-sky views so as to calibrate the reference radiometer (NIR) by the so-called one-point calibration [9]. If η_2 and η_1 are NIR readings when acting as the reference radiometer to measure the HOT and WARM injected noise (Fig. 1), respectively, we can write

$$T_{N2} = \frac{\eta_2 - \eta_{\rm off}}{G_N^C} \qquad T_{N1} = \frac{\eta_1 - \eta_{\rm off}}{G_N^C} \tag{16}$$

where G_N^C and $\eta_{\rm off}$ are NIR offset and gain at plane C (NDN output). For any LICEF in measurement mode, system noise at the antenna plane can be expressed by combining (3), (8), (9), and (16) into

$$T_{\rm sys}^{A_k} = \frac{v_k^A - v_{{\rm off}k}}{v_{2k} - v_{1k}} \frac{|S_{k0}|^2}{|S_{n0}|^2} \frac{|S_{LC_k}|^2}{|S_{LA_k}|^2 \eta_{A_k}} \frac{\eta_2 - \eta_1}{G_N^C}. \tag{17}$$

As derived from (17), absolute calibration accuracy mainly depends on the error in the estimation of NIR gain, antenna losses, and relative S-parameter amplitude. The NDN is designed to minimize differential dispersion due to temperature gradients. In-orbit thermal monitoring shall constrain the NDN S-parameter error to the required ± 0.045 dB. As will be shown in the following sections, ground-measured NDN S parameters can also be retrieved during deep-sky imaging, so as to validate the calibration scheme.

A. PMS One-Point Calibration

In order to validate the in-orbit calibration approach, the PMS can be calibrated during deep-sky views by a similar strategy of that applied to calibrate the NIR. Note that the PMS can be calibrated at the antenna plane either to measure system temperatures or antenna temperatures

$$\begin{aligned} v_A &= G^A T_{{\rm sys}_A} + v_{\rm off} = G^A T_A + v'_{\rm off} \\ v'_{\rm off} &= v_{\rm off} + G^A T_{\rm R}^A. \end{aligned} \tag{18}$$

It must be pointed out that PMS gain is the same in both cases. $T_{\rm R}^A$ is the equivalent receiver temperature referred to as the antenna plane. For the sake of simplicity and without loss of generality, we can consider $v_{\rm off} = 0$ (it can be measured and canceled out independently by the four-point method if required). Now, the equivalent system temperature at the antenna plane, when the switch in Fig. 10 is in position U (WARM) or A (COLD), can be expressed as

$$\begin{aligned} T_{\rm sysW}^A &= \frac{1}{\eta_A |S_{LA}|^2} (T_{\rm ph} + T_{\rm rec}) \\ T_{\rm sysC}^A &= T_{\rm sky} + \frac{T_{\rm ph}\left(1 - \eta_A |S_{LA}|^2\right) + T_{\rm rec}}{\eta_A |S_{LA}|^2}. \end{aligned} \tag{19}$$

The WARM and COLD PMS readings are, respectively, given by

$$v_{\rm W} = G^A T_{\rm sysW}^A \qquad v_{\rm C} = G^A T_{\rm sysC}^A. \tag{20}$$

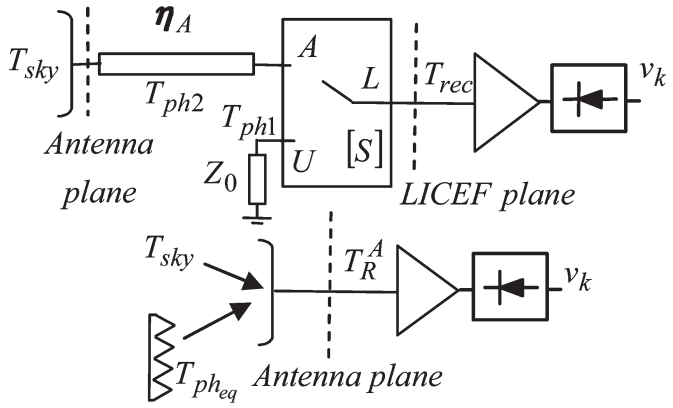

Fig. 10. PMS front-end scheme to illustrate the one-point calibration. The equivalent model for the differential system and antenna temperatures $T_{\rm ph} - T_{\rm sky} = T^A_{\rm sysW} - T^A_{\rm sysC}$.

Then, PMS gain can be calculated as

$$G^A = \frac{v_{W-}v_{\rm C}}{T^A_{\rm sysW} - T^A_{\rm sysC}}. \tag{21}$$

System temperatures are unknown; however, in this case it holds

$$T^A_{\rm sysW} - T^A_{\rm sysC} = T_{\rm ph} - T_{\rm sky} \tag{22}$$

and the gain can be estimated as

$$G^A = \frac{v_{\rm W-}v_{\rm C}}{T_{\rm ph} - T_{\rm sky}}. \tag{23}$$

Now, PMS offset is directly retrieved as

$$v'_{\rm off} = \frac{v_{\rm C}T_{\rm ph} - v_{\rm W}T_{\rm sky}}{T_{\rm ph} - T_{\rm sky}} \tag{24}$$

which also holds in the case that $v_{\rm off} \neq 0$. As a conclusion, one-point calibration allows to calibrate the PMS to give both system temperature and antenna temperature, without the need for an external warm target. Additionally, it is worth to mention that in the case that the switch and the antenna are at different temperatures, the contribution of thermal noise at the front end can be taken into account if $T_{\rm ph1}$, $T_{\rm ph2}$, and η_A are measured. The calibration still holds by substituting $T_{\rm ph}$ for an equivalent physical temperature at the antenna plane given by

$$T^A_{\rm ph_{eq}} = \frac{T_{\rm ph1} - T_{\rm ph2}}{\eta_A} + T_{\rm ph2}. \tag{25}$$

Moreover, assuming that antenna losses are estimated with an error $\hat{\eta}_A = \eta_A(1 + \delta_A)$, then the error in the estimation of the equivalent physical temperature is

$$\delta T^A_{\rm ph_{eq}} = \frac{T_{\rm ph1} - T_{\rm ph2}}{\eta_A}\delta_A \tag{26}$$

i.e., the fractional error of antenna losses has a low impact on the calibration, since it is multiplied by the difference of two similar physical temperatures.

Finally, the PMS can also be fully calibrated by the one-point method to measure antenna temperature, since combining (23) and (24) yields

$$T^A_{\rm R} = \frac{v_{\rm C}T_{\rm ph_{eq}} - v_{\rm W}T_{\rm sky}}{v_{\rm W} - v_{\rm C}}. \tag{27}$$

B. In-Orbit Calibration of the NDN

In the previous section, PMS gain is calibrated by means of the one-point external calibration during deep-sky views. However, a second estimation of PMS gain can also be obtained by the internal calibration. The PMS gain at the antenna plane can be written from (17) as

$$G^A_k = G^{CA}_N \frac{v_{2k} - v_{1k}}{\eta_{N2} - \eta_{N1}} \frac{B_k}{B_n} \tag{28}$$

where the NIR gain at the C plane G^C_N has been translated to the NIR antenna plane G^{CA}_N in a similar way as that done for the PMS. The parameter B_k is defined as the transmission parameter from antenna k plane to the input of the NDN (port "0")

$$B_k = \frac{|S_{LA_k}|^2}{|S_{LC_k}|^2} \frac{\eta_{A_k}}{|S_{k0}|^2}. \tag{29}$$

A similar expression B_n holds for the transmission parameter from the NIR antenna plane to the input of the NDN. Then, combining (23) and (28), the transmission coefficients, relative to the NIR path, relating each PMS can be retrieved

$$\frac{B_k}{B_n} = \frac{1}{G^{CA}_N} \frac{\eta_2 - \eta_1}{T_{\rm ph_k} - T_{\rm sky_k}} \frac{v_{kW-}v_{kC}}{v_{2k} - v_{1k}}. \tag{30}$$

This expression, which is exclusively computed from calibration measurements during deep-sky views, can now be compared to the value estimated from ground measurements (after temperature correction)

$$\frac{B_k}{B_n} = \frac{|S_{LA_k}|^2}{|S_{LC_k}|^2} \frac{\eta_{A_k}}{|S_{k0}|^2} \frac{|S_{LC_n}|^2}{|S_{LA_n}|^2} \frac{|S_{n0}|^2}{\eta_{A_n}}. \tag{31}$$

Note that the term B_k/B_n simply represents the unbalance of the calibration network path to each PMS antenna plane, relative to the NIR path. It would value one for a perfectly balanced instrument. The procedure described so far is intended to provide, during deep-sky views, a validation of the PMS calibration procedure by internal calibration. Of course, (30) also holds during the observation mode just changing the sky temperature by the antenna temperature when looking at the Earth. However, in this last case, the errors will be much larger due to the reduced difference between the calibration temperatures and a larger error in the estimation of antenna temperature.

C. PMS Linearity Correction

Finally, PMS nonlinearity affects the accuracy of absolute calibration. In [7], it was shown that the PMS behavior is very well modeled by means of a second-order response

$$v_k = v_{\mathrm{off}k} + G_k^C T_{\mathrm{sysC}k} + a_k [T_{\mathrm{sysC}k}]^2. \tag{32}$$

The second-order term is measured by means of the so-called deflection or slope method [10], [11], yielding a value close to $a_k = 5 \cdot 10^{-6}$ mV/K^2. This gives a maximum error due to nonlinearity of about 1%, defined as the maximum fractional error in the estimation of system temperature for antenna temperatures ranging from 2.7 to 300 K (observation mode). The error is computed when PMS gain and offset are calibrated by the four-point method with the HOT and WARM temperatures described in Section I-A. This error can be reduced for in-orbit estimations of system temperature (both in measurement or calibration mode) by using the ground-measured second-order term as

$$T_{\mathrm{sys}k} = \frac{v_k^c - v_{\mathrm{off}k}}{G_k} \tag{33}$$

where the linearity-corrected PMS voltage v_k^c is given by

$$v_k^c = v_k - a_k \left[T_{\mathrm{sys}k}^i\right]^2. \tag{34}$$

v_k are direct PMS voltage readings. The first estimation of system temperature is computed as

$$T_{\mathrm{sys}k}^i = \frac{v_k - v_{\mathrm{off}k}^i}{G_k^i} \tag{35}$$

where $v_{\mathrm{off}k}^i$ and G_k^i are first estimates of the related magnitudes by neglecting the second-order term. This second-order term is assumed to have low aging and temperature drift. Anyway, the major advantage of this iterative method is given by the fact that it is very robust in front of error in the estimation of a_k: the error in the estimation of $T_{\mathrm{sys}k}$ can be reduced below 0.1% even in the case that the error in the estimation of a_k is about $\pm 10\%$.

IV. Conclusion

The relative and absolute amplitude calibration of the MIRAS–SMOS instrument has been reviewed taking into account the experimental results from the first batch of engineering model receivers, which are fully representative of the flight hardware. Experimental results have shown state-of-the art baseline performance and the capability of the system to be calibrated in orbit to compensate for temperature thermal drift. Residual errors after calibration are well below system specifications: 1% for the amplitude, 1° for the phase, and 1 c.u. for the offset. A method to validate the relative calibration of the instrument during deep-space views has also been sketched. This validation is based on one-point calibration of the PMS as developed in this paper. Additionally, a proposal to reduce PMS linearity errors to 0.1% has also been proposed.

The experimental results presented in this paper are related to the MIRAS–SMOS hardware. However, they give a very good grasp on state-of-the art single-baseline performance, which is the core of any passive interferometer devoted to remote sensing. Quantitative measurements on what can be achieved in terms of stability and temperature sensitivity of complex normalized and denormalized correlations, offset noise, or fringe washing response are presented. The differences between nominal and redundant correlation and fringe wash terms show the impact of small differences in the frequency response of the in-phase and quadrature branches. Finally, the results reveal that the dominant source of error, by far, comes from the amplitude denormalization of the correlations. An interesting result, indeed, since it has been widely believed that the use of one-bit two-level correlators made the interferometer insensitive to amplitude changes.

Acknowledgment

The LICEF receivers and measurement setup were manufactured by Mier Comunicaciones, Space Department, La Garriga, Spain, in the frame of the SMOS project. All measurements were also performed by Mier Comunicaciones.

References

[1] Y. H. Kerr, P. Waldteufel, J. P. Wigneron, J. M. Martinuzzi, J. Font, and M. Berger, "Soil moisture retrieval from space: The Soil Moisture and Ocean Salinity (SMOS) mission," *IEEE Trans. Geosci. Remote Sens.*, vol. 39, no. 8, pp. 1729–1735, Aug. 2001.

[2] J. Font, G. Lagerloef, D. LeVine, A. Camps, and O. Z. Zanife, "The determination of surface salinity with the European SMOS space mission," *IEEE Trans. Geosci. Remote Sens.*, vol. 42, no. 10, pp. 2196–2205, Oct. 2004.

[3] M. Martin-Neira and J. M. Goutule, "A two-dimensional aperture synthesis radiometer for Soil Moisture and Ocean Salinity observations," *ESA Bull.*, no. 92, pp. 95–104, Nov. 1997.

[4] I. Corbella, F. Torres, A. Camps, A. Colliander, M. Martín-Neira, S. Ribó, K. Rautiainen, N. Duffo, and M. Vall-llossera, "MIRAS end-to-end calibration: Application to SMOS L1 processor," *IEEE Trans. Geosci. Remote Sens.*, vol. 43, no. 5, pp. 1126–1134, May 2005.

[5] I. Corbella, F. Torres, A. Camps, N. Duffo, M. Vall-llossera, and M. Martin-Neira, "Baseline calibration of interferometric radiometers: Experimental results," in *Proc. IGARSS*, Seoul, Korea, Jul. 2005, pp. 5547–5550.

[6] P. Piironen, "PMS offset determination using an IF attenuator," ESA-ESTEC, Noordwijk, The Netherlands, Tech. Note 14629/00/NL/SF, Jun. 2002.

[7] F. Torres, N. Duffo, I. Corbella, A. Camps, M. Vall-llossera, and L. Sagués, "Dynamic range and linearity tradeoff in detectors for interferometric radiometers," *Electon. Lett.*, vol. 39, no. 25, pp. 1852–1854, Dec. 11, 2003.

[8] I. Corbella, A. Camps, F. Torres, and J. Bara, "Analysis of noise-injection networks for interferometric-radiometer calibration," *IEEE Trans. Microw. Theory Tech.*, vol. 48, pt. 1, no. 4, pp. 545–552, Apr. 2000.

[9] A. Colliander, S. Tauriainen, T. Auer, J. Uusitalo, M. Toikka, and M. Halikainen, "Evaluation of in-orbit temperature variation on performance of MIRAS prototype noise injection radiometer," in *Proc. IGARSS*, Sep. 20–24, 2004, vol. 2, pp. 781–784.

[10] F. A. Pellerano, K. H. Horgan, W. J. Wilson, and A. B. Tanner, "Development of a high-stability microstrip-based L-band radiometer for ocean salinity measurements," in *Proc. IGARSS*, Sep. 2004, vol. 2, pp. 774–776.

[11] N. Skou, "Microwave radiometer linearity measured by simple means," in *Proc. IGARSS*, Jun. 2002, vol. 6, pp. 3664–3667.

Francesc Torres (S'88–M'96) was born in Ibiza, Spain, in 1962. He received the Ingeniero and Doctor Ingeniero degrees in telecommunication engineering from the Polytechnic University of Catalonia (UPC), Barcelona, Spain, in 1988 and 1992, respectively.

From 1988 to 1989, he was a Research Assistant in the RF System Division at the European Space Agency devoted to microwave device testing and characterization. In 1989, he joined the Antenna-Microwave-Radar group of UPC, where he currently holds a post as Assistant Professor. From 2005 to 2006, he has been holding a sabbatical year in the Microwave Systems Section of the Jet Propulsion Laboratory, Pasadena, CA. His main research interests include the design and test of microwave systems and subsystems. He is currently engaged in research on interferometric radiometers devoted to Earth observation.

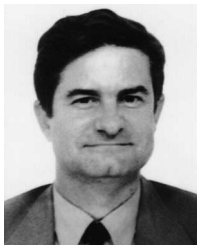

Ignasi Corbella (M'99) received the degree in telecommunications engineering and Doctor Engineering degree from the Universitat Politècnica de Catalunya (UPC), Barcelona, Spain, in 1977 and 1983, respectively.

In 1976, he joined the School of Telecommunication Engineering in UPC as a Research Assistant in the Microwave Laboratory, were he worked on passive-microwave integrated circuit design and characterization. In 1979, he worked at Thomson-CSF, Paris, France, on microwave oscillator design. In 1982, he became an Assistant Professor at UPC, an Associate Professor in 1986, and a Full Professor in 1993. He is currently teaching microwaves at the undergraduate level in UPC and has designed and taught graduate courses on nonlinear microwave circuits. During the school year 1998–1999, he worked at the NOAA/Environmental Technology Laboratory, Boulder, CO, as a Guest Researcher, developing methods for radiometer calibration and data analysis. His research work in the Department of Signal Theory and Communications, UPC, includes microwave airborne and satellite radiometry and microwave system design.

Adriano Camps (S'91–A'97–M'00–SM'03) was born in Barcelona, Spain, in 1969. He received the degree in telecommunications engineering and the Ph.D. degree in telecommunications engineering both from the Polytechnic University of Catalonia (UPC), Barcelona, in 1992 and 1996, respectively.

From 1991 to 1992, he was with the ENS des Télécommunications de Bretagne, Bretagne, France, with an Erasmus Fellowship. In 1993, he joined the Electromagnetics and Photonics Engineering group, at the Department of Signal Theory and Communications, UPC, as an Assistant Professor, and since 1997, as an Associate Professor. In 1999, he was on sabbatical leave at the Microwave Remote Sensing Laboratory, University of Massachusetts, Amherst. His research interests are microwave remote sensing, with special emphasis on microwave radiometry by aperture synthesis techniques. He has performed numerous studies within the frame of the European Space Agency (ESA) SMOS Earth Explorer Mission. He is an Associate Editor of *Radio Science*.

Dr. Camps received the second national award of university studies in 1993; the INDRA award of the Spanish Association of Telecommunication Engineering to the best Ph.D. in 1997; the extraordinary Ph.D. award at the Universitat Politècnica de Catalunya in 1999; the First Duran Farell Award and the Ciudad de Barcelona Award, in 2000 and 2001, respectively, both for Technology Transfer; and the Research Distinction of the Generalitat de Catalunya for contributions to microwave passive remote sensing in 2002. He also won the "Premi Nacional de Telecomunicacions 2003" and "Premi Salvà i Campillo 2004." He was the Chair of Cal '01. He is the Editor of the IEEE GEOSCIENCE AND REMOTE SENSING Newsletter and President–Founder of the IEEE GEOSCIENCE AND REMOTE SENSING Society Chapter in Spain.

Núria Duffo (S'91–M'99) received the degree in telecommunication engineering degree and the Doctor in telecommunication engineering degree from the Polytechnic University of Catalonia (UPC), Barcelona, Spain, in 1990 and 1996, respectively.

Since 1997, she has been an Associate Professor at UPC. Her current research interests are in numerical methods in electromagnetics, microwave radiometry, antenna analysis, and design.

Mercè Vall-llossera (M'99) received the senior telecommunication engineer and the Doctor telecommunication engineering degrees from the Polytechnic University of Catalonia (UPC), Barcelona, Spain, in 1990 and 1994, respectively.

She has been lecturing and doing research at the Department of Signal Theory and Communications, UPC, from 1990 until 1997 as an Assistant Professor, and since 1997, as an Associate Professor. She spent a sabbatical year in Montreal with the scholarship of the "Programme Québécois de Bourses d'Excellence" (1996–1997): "Stages de Formation postdoctorale au Québec pour jeunes diplômés étrangers." Her research interests include numerical methods in electromagnetism, microwave radiometry, antenna analysis, and design. Currently, her research is mainly related to the study of numerical methods applied to sea surface emissivity and their characterization at L-band and the MIRAS/SMOS project.

Dr. Vall-llossera, along with the other member of the radiometry group at UPC, was awarded the "Primer Premio Duran Farell de Investigación Tecnológica" in 2002, the "Primer Premio Ciutat de Barcelona d'Investigació Tecnològica" in 2001, the "Premi Nacional de Telecomunicacions 2003," and the "Premi Salvà i Campillo 2004."

Santiago Beraza was born in Zaragoza, Spain, in 1980. He received the degree in telecommunication engineering from the Universidad de Zaragoza, Zaragoza, in 2004. He is currently working toward the Ph.D. degree at the Universitat Politècnica de Catalunya (UPC), Barcelona, Spain.

Since September 2002, he has been at UPC. In February 2004, he joined the Department of Signal Theory and Communications, UPC. He has been involved in some test and field campaigns within the frame of the ESA's SMOS mission.

Carles Gutiérrez received the degree in telecommunications engineering from the Polytechnic University of Catalonia (UPC), Barcelona, Spain, in 2005.

In 2004, as an undergraduate student, he received from UPC a grant to work on interferometric radiometers with the Department of Signal Theory and Communications, UPC.

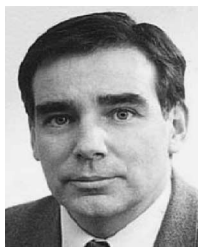

Manuel Martín-Neira (M'96) received the M.S. and Ph.D. degrees in telecommunication engineering from the Polytechnic University of Catalonia (UPC), Catalonia, Spain, in 1986 and 1996, respectively.

From 1989 to 1992, he was with GMV, a Spanish firm, where he was responsible for several projects for the European Space Agency (ESA) related to global positioning satellite navigation with applications to precise landing and attitude determination. Since 1992, with ESA, he has been in charge of the radiometer activities within the Payload Equipment and Technology Section. During this period, he has been responsible for the aperture synthesis MIRAS project.

Dr. Martín-Neira was awarded a Fellowship to work on radiometry at the European Space Research and Technology Center (ESTEC), Noordwijk, The Netherlands, in 1988.